Supplemental Material for

"Bubble cloud nucleation induced by a pair of laser-induced shocks and bubbles"

Pedro A. Quinto-Su and Keita Ando

(Received)

Physical model

Multicomponent Euler equations in two-dimensional axisymmetric configuration (Johnsen & Colonius 2008, 2009) are used to describe the interaction of two laser-induced bubbles in water. A pressure jump across interfaces of the bubbles of concern (i.e., Laplace pressure due to surface tension) is so small (compared to the initial bubble pressure) that surface tension is ignored in the modelling. The Euler equations are closed with the stiffened equation of state (Cocchi *et al.* 1996):

$$\frac{P}{\gamma-1}+\frac{\gamma P'_\infty}{\gamma-1}=E-\frac{\rho}{2}(\mathbf{u}\cdot\mathbf{u}),$$

where P is the pressure, E is the total energy per unit volume, ρ is the density, $\mathbf{u}$ is the velocity vector, and γ and P'_∞ are stiffness and tensile strength, respectively, of the fluid. For gases with $P'_\infty = 0$ (i.e., no cohesion between gas molecules), this reduces to the ideal gas law. The expansion of laser-induced bubbles is treated as ideal gases; the implication is that the bubble expansion rate is much larger than the evaporation rate at the bubble wall so that the bubble contents tend to behave as noncondensible gases.

With the stiffened equation, the speed of sound is given by $c = \sqrt{\gamma(P+P'_\infty)/\rho}$. For gases, γ thus stands for the ratio of adiabatic heats. For liquids, the specification of both γ and P'_∞ is required to define the speed of sound. The value of γ varies between previous studies on shock calculations in water, but its selection does not have an impact on numerical solutions for expanding bubbles whose initial pressure is up to 6 GPa (Ando *et al.* 2012). Here, we select $\gamma = 7.15$, which is commonly used in shock calculations for water (Thompson 1972). With c specified at room temperature, the value of P'_∞ is therefore determined.

The initial pressure of the laser-induced bubble at time $t = 0$ are selected to obtain reasonable agreement with the measured evolution of the shock front and the bubble wall. Now that the initial expansion is assumed so rapid that the bubble behaves adiabatically (Aitken *et al.* 1996), the initial bubble density ρ_i obeys $\rho_i = \rho_0(P_i/P_0)^{1/\gamma}$ where ρ_0 is set to the density of water vapor at room temperature (20°C), P_0 denotes one atmosphere, and P_i is the initial bubble pressure to be tuned to reproduce the measurement.

Numerical simulation

To accurately capture both shocks and bubble interfaces, the advection equations for γ and P'_∞ as well as the Euler equations are solved using the finite volume method proposed by Johnsen and Colonius (Johnsen & Colonius 2006). A third-order Runge–Kutta scheme designed for robust calculations (Shu & Osher 1988; Gottlieb & Shu 1998) is used for time marching. The computational grid is based on two-dimensional Cartesian coordinates with uniform grid spacing of $0.04R_0$ where the initial bubble radius R_0 is set to 8 μm. The computational domain is large enough that spurious waves, which can be generated at the computational boundaries, do not contaminate the solution of concern. It is confirmed that with this grid resolution and sufficiently small time step (for stable integration), the evolution of the simulated shocks and bubbles is well converged and indistinguishable from that with a double grid resolution.

Figure S1 presents the simulated evolution of the two expanding bubbles whose initial separation is 50.9 μm (corresponding to the left column of figure 2 in the main text). To achieve agreement in the evolution of the pressure waves and the bubble interface, the initial pressure of the laser-induced bubbles is set to 2 GPa. In the pressure plot, the nominal location of the bubble interfaces (white lines) is defined as the contour of $\gamma = 4.2$. To detail the interaction between the pressure waves and the bubble interfaces, the movie of the pressure distribution along the axis of symmetry (up to 60 ns) can be found in `xpres_upto60ns.mov` in which blue and red lines stand for the pressure and the bubble wall location, respectively. The spherical shocks collide, producing a sharp pressure rise (9 ns). The shocks reach the interface of the opposing bubbles and reflect as tension waves due to acoustic impedance mismatch (14 ns). Because of superposition of the reflected tensions and the still incoming tail of the shock, the extent of tension in the liquid neighbouring the bubble surface is rather weak. The reflected tension waves meet and the water starts to be stretched (19 ns). These tension waves

again reach the expanding bubbles and reflect now as compression waves, which are to drive the collapse of the nucleated bubbles observed in the experiment (34 ns). During the observation period, the laser-induced bubbles are still under expansion, but deform due to the interaction (59 ns).

REFERENCES

Aitken, F., McCluskey, F. M. J. & Denat, A. 1996 An energy model for artificially generated bubbles in liquids. *J. Fluid Mech.* **327**, 373–392.

Ando, K., Liu, A. Q. & Ohl, C. D. 2012 Homogeneous nucleation in water in microfluidic channels. *Phys. Rev. Lett.* **109**, 044501.

Cocchi, J. P., Saurel, R. & Loraud, J. C. 1996 Treatment of interface problems with Godunov-type schemes. *Shock Waves* **5**, 347–357.

Gottlieb, S. & Shu, C.-W. 1998 Total variation diminishing Runge-Kutta schemes. *Math. Compt.* **67**, 73–85.

Johnsen, E. & Colonius, T. 2006 Implementation of WENO schemes in compressible multicomponent flow problems. *J. Comput. Phys.* **219**, 715–732.

Johnsen, E. & Colonius, T. 2008 Shock-induced collapse of a gas bubble in shockwave lithotripsy. *J. Acoust. Soc. Am.* **124**, 2011–2020.

Johnsen, E. & Colonius, T. 2009 Numerical simulations of non-spherical bubble collapse. *J. Fluid Mech.* **629**, 231–262.

Shu, C.-W. & Osher, S. 1988 Efficient implementation of essentially non-oscillatory shock-capturing schemes. *J. Comput. Phys.* **77**, 439–471.

Thompson, P. A. 1972 *Compressible-Fluid Dynamics*. McGraw-Hill.

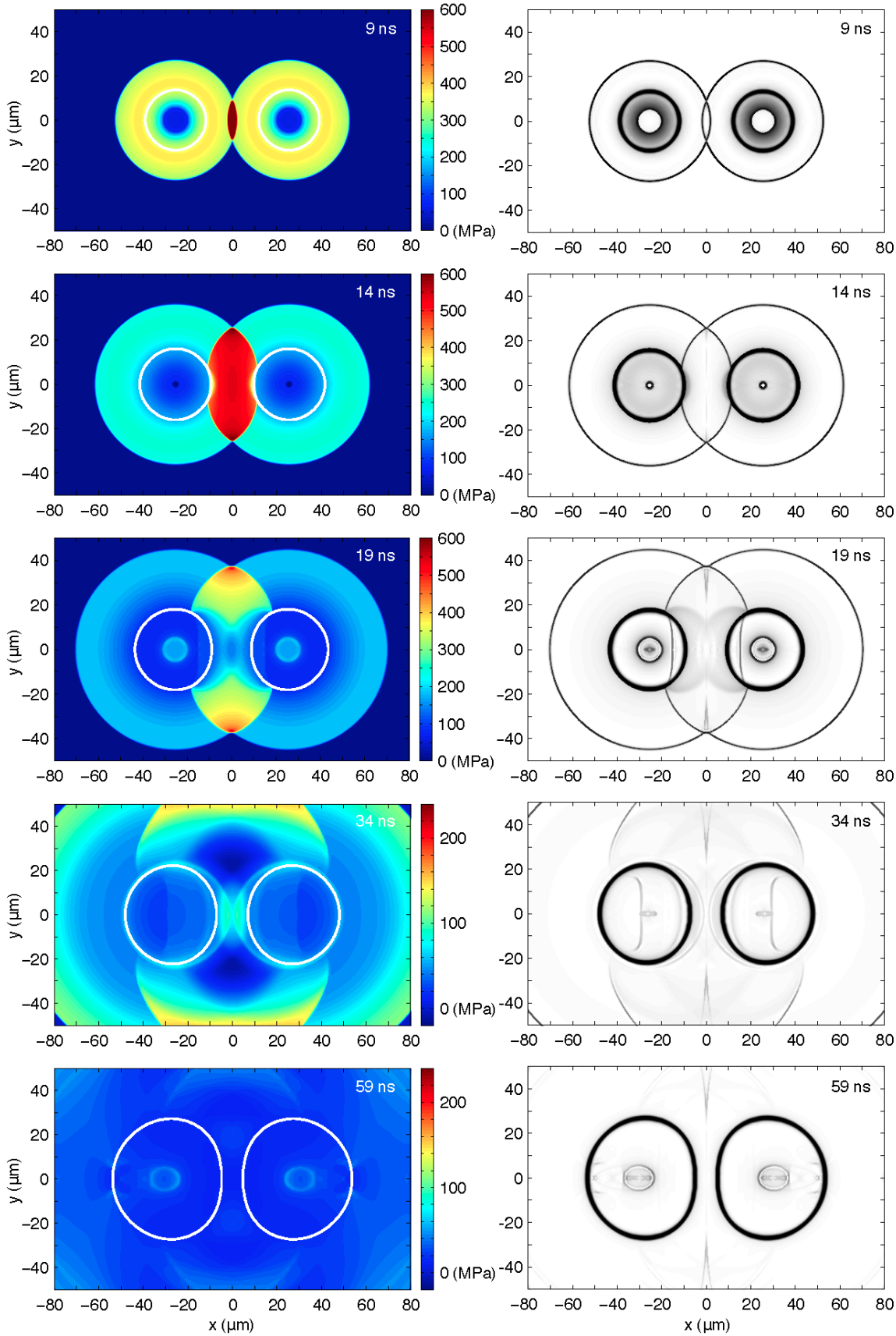

Figure S1. Evolution of the simulated pressure distribution (left) and numerical Schlieren (right) corresponding to figure 2 with $d = 50.9$ μm in the main text. For the pressure evolution along the axis of symmetry, see `xpres_upto60ns.mov`.